PCCP

Accepted Manuscript

This article can be cited before page numbers have been issued, to do this please use: A. Striolo, A. Phan, T. Bui, E. Acosta and P. Krishnamurthy, *Phys. Chem. Chem. Phys.*, 2016, DOI: 10.1039/C6CP03296F.

ROYAL SOCIETY OF CHEMISTRY

www.rsc.org/pccp

View Article Online
DOI: 10.1039/C6CP03296F

Molecular Mechanisms Responsible for Hydrates Anti-Agglomerants Performance

Anh Phan[#], Tai Bui[#], Erick Acosta[+], Pushkala Krishnamurthy[+] and Alberto Striolo[#]

[#] Department of Chemical Engineering, University College London, WC1 E7JE London, UK

[+] MultiChem, a Halliburton Service, Houston, Texas, USA

Abstract

Steered and equilibrium molecular dynamics simulations were employed to study the coalescence of a sI hydrate particle and a water droplet within a hydrocarbon mixture. The size of both the hydrate particle and the water droplet is comparable to that of the aqueous core in reverse micelles. The simulations were repeated in the presence of various quaternary ammonium chloride surfactants. We investigated the effects due to different groups on the quaternary head group (e.g., methyl vs. butyl groups), as well as different hydrophobic tail lengths (e.g., n-hexadecyl vs. n-dodecyl tails) on the surfactants ability to prevent coalescence. Visual inspection of sequences of simulation snapshots indicates that when the water droplet is not covered by surfactants it is more likely to approach the hydrate particle, penetrate the protective surfactant film, reach the hydrate surface, and coalesce with the hydrate than when surfactants are present on both surfaces. Force – distance profiles obtained from steered molecular dynamics simulations and free energy profiles obtained from umbrella sampling suggest that surfactants with butyl tripod on the quaternary head group and hydrophobic tails with size similar to the solvent molecules can act as effective anti-agglomerants. These results qualitatively agree with macroscopic experimental observations. The simulation results provide additional insights, which could be useful in flow assurance applications: the butyl tripod provides adhesion between surfactants and hydrate; when the length of the surfactant tail is compatible with the hydrocarbon in the liquid phase a protective film can form on the hydrate; however, once a molecularly thin chain of water molecules forms through the anti-agglomerants film, connecting the water droplet and the hydrate, water flows to the hydrate and coalescence is inevitable.

* Author to whom correspondence should be addressed: a.striolo@ucl.ac.uk

View Article Online
DOI: 10.1039/C6CP03296F

Introduction

Clathrate hydrates, also known as gas hydrates, are inclusion compounds created by hydrogen-bonded water stabilized by embedded guest molecules (e.g., methane, ethane, propane or carbon dioxide).[1] Gas hydrates have seized a lot of attention from both industrial and academic communities[2-5] because of the potential of harvesting natural gas as an energy source from hydrates deposits,[6] which need to be conducted carefully to avoid environmental consequences,[4,6-8] as well as a possible solution for long-term storage of carbon dioxide. Hydrates also pose a significant problem for the oil and gas industry, specifically in flow assurance: already in 1934 Hammerschmidt pointed out that natural gas hydrates were blocking gas transmission lines.[9] Pipeline blockage should be avoided, as it can lead to (1) environmental and safety consequences due to pipeline bursting, and (2) significant financial losses due to the interruption of well production.[9] Currently, hydrates are managed in flow assurance via the use of chemical inhibitors.[10,11] In general, two kinds of inhibitors can be used: (1) thermodynamic inhibitors (THIs) typically used in large quantities (up to 50 vol%),[10,12] and (2) low-dosage hydrate inhibitors (LDHIs) effective at low concentrations (0.5 wt%).[10] LDHIs include kinetic hydrate inhibitors (KHIs) and anti-agglomerants (AAs).[10,11] KHIs play a role of disrupting the water – water hydrogen bonding network and then restricting the hydrate formation while AAs prevent the aggregation of hydrate particles and thus make it possible, under appropriate conditions, to transport the hydrate-containing slurry. AAs, surface-active chemicals, typically show better performance than KHIs at high sub-cooling conditions, but require the presence of a liquid hydrocarbon phase for proper performance. AAs typically contain hydrophobic tails, sometimes branched, and one extended hydrate-philic head. The first class of AAs was patented by Shell[13] and research since then has generated several additional classes of chemistries.[14] Although a large number of experimental studies[15-24] have been conducted to investigate AAs, their mechanism of action is not completely understood. Understanding how the AAs molecular structure affects performance can lead to designing new AAs formulations.

Building on the fundamental understanding of the kinetics of colloidal coalescence available in the literature,[25-30] we employ steered and equilibrium molecular dynamics (MD) simulations to investigate

View Article Online
DOI: 10.1039/C6CP03296F

the coalescence of a sI hydrate particle and a water droplet embedded in a hydrocarbon mixture (n-decane and methane). Although the available computing-power limits the system size that can be investigated at the atomistic level, the size of both the water droplet and the hydrate particle is comparable to that of the aqueous core in reverse micelles. As such, the simulated system could be representative of the coalescence of emulsified water micro-droplets with just-nucleated hydrate particles. We investigate how various quaternary ammonium chloride surfactants affect the mechanism of coalescence. All calculations are performed at the atomistic length scale. We consider different groups on the quaternary head group of the surfactants (e.g., methyl vs. butyl groups), as well as different hydrophobic tail lengths (e.g., n-hexadecyl vs. n-dodecyl tails). We attempt to relate the molecular properties of the surfactants, considered as AAs in our model study, to the mechanism of coalescence between hydrate particle and water droplet, which we interpret as a molecular-scale signature of macroscopic performance in hydrate management. Future investigations will clarify how the curvature of the interfaces (both that of the water droplet and that of the hydrate particle) affects the molecular mechanisms of coalescence. The simulations are analyzed in an effort to unveil molecular mechanisms that could be exploited to control the performance of anti-agglomerants. Some of the results agree with general expectations, suggesting for example that strong adhesion between the surfactants head groups and the hydrate particles should improve performance. Others are less expected, suggesting for example that cohesion between the hydrophobic tail groups to yield a protective film impervious to water could be a useful feature of surfactants used in flow assurance.

Simulation Methodology

Steered and equilibrium molecular dynamics (MD) simulations were performed using the package GROMACS.[31,32] The simulations were conducted at the atomistic level.

One representative simulation set up is reproduced in Figure 1. Each simulated system contains one hydrate particle, one water droplet, and surfactants, all immersed in a hydrocarbon mixture. The hydrocarbon phase contains n-decane and methane. The hydrate particle of ~1.5 nm in radius was carved out of the bulk structure of sI methane hydrate. We maintained all atoms in the hydrate particle

View Article Online
DOI: 10.1039/C6CP03296F

rigid, as we are not focusing on the stability of the hydrate. Additional simulations, not included in this contribution for brevity, conducted for a flat hydrate substrate in contact with a hydrocarbon phase, in which the molecules in the hydrate were not maintained rigid, show that a sub-molecular layer of water molecules can form at the hydrate-hydrocarbon interface. Such layer could in principle introduce defects on the hydrate cages, which could alter the strength of adsorption of the surfactants on the hydrate. Such effects are not expected to alter the conclusions of the present research, focused on the mechanism by which surfactants can prevent the agglomeration between a water droplet and a hydrate particle. The observations just briefly mentioned are being quantified systematically and will be discussed in a future report.

In the simulations presented here the hydrate particle was covered with single-tail quaternary ammonium chloride surfactants. We simulated three such surfactants: n-hexadecyl-trimethyl-ammonium chloride (C16C1), n-hexadecyl-tri(n-butyl)-ammonium chloride (C16C4), and n-dodecyl-tri(n-butyl)-ammonium chloride (C12C4). Their molecular structures are shown in Figure 2. The water droplet was prepared by extracting a sphere out of bulk liquid water; it was 1.25 nm in radius. The size of the water droplet was chosen to be comparable to the aqueous core of reverse micelles obtained by dispersing water in decane in the presence of surfactants.[33] The water droplet was either covered by surfactants (the same surfactants used for the hydrate particle) or not. We refer to the two cases as coated and bare droplet, respectively. The amount of surfactants used to cover both the water droplet and the hydrate particle was determined using experimental data available regarding the ratio between molar concentration of water and that of surfactants in reverse micelles obtaining dispersing water in decane. This ratio is estimated in ~ 7-8 for reverse micelles with aqueous core radius comparable to that used in the present simulations.[33,34]

To build each simulated system we first deposited 87 surfactants on the hydrate particle and 48 surfactants on the water droplet (this was not necessary for the bare droplet case) and we equilibrated the two systems (particle and droplet) separately at 277 K for 10 ns. The amounts of surfactants were sufficient to achieve a surface density of ~ 3.1 molecules/nm^2 and ~ 2.5 molecules/nm^2 on the hydrate particle and on the water droplet, respectively. We then inserted hydrate particle and water droplet, together with the desired amount of n-decane and methane molecules, in a rectangular simulation cell

View Article Online
DOI: 10.1039/C6CP03296F

of dimensions 9.09 nm × 10.60 nm × 17.44 nm (bare droplet) or 9.15 nm × 10.67 nm × 17.55 nm (coated droplet). In all cases, the n-decane : methane : water molar composition was of 7 : 0.44 : 2.5. From the initial configuration just described, we first conducted simulations in the canonical ensemble (NVT) (constant number of particles, volume, and temperature) for 5ns at T= 277 K, followed by simulations in the NPT ensemble (constant number of particles, pressure, and temperature) at P = 10 MPa and T = 277 K. Once the total system energy and the volume stabilized (within ~ 200 ps), we progressed the simulations in the NVT ensemble for additional 30 ns. This procedure was considered adequate to yield equilibrated configurations because the bulk density of n-decane approached the experimental bulk liquid density at the thermodynamic conditions chosen for the simulations. The equilibrated systems were used as initial configurations for the steered simulations to investigate the coalescence. The results presented below for both equilibrium and steered simulations were obtained at thermodynamic conditions (T = 277 K and P = 10 MPa) favorable for hydrate formation.[4]

The Transferable Potentials for Phase Equilibria force field in the united-atom form (TraPPE-UA)[35] was implemented to describe n-decane and methane. The potential parameters developed by Jorgensen and Gao[36] were used to model the surfactant quaternary head group while the tail alkyl groups were described by the force field from Smit et al.[37] These force fields are known to yield good agreement with experimental data in terms of the hydration properties of the ammonium compounds and of the critical properties for alkanes, respectively.[36,37] The rigid SPC/E model was used to simulate water molecules both in the droplet and in the sI hydrate.[38] The SPC/E water bonds and angles were kept fixed by employing the SETTLE algorithm.[39] Although the SPC/E model does not describe satisfactorily the solid-liquid phase diagram of water, we have used it previously to quantify liquid water properties at interfaces in the presence of surfactants.[40,41] Good agreement was for example obtained with experimental data for the thickness of $C_{12}E_6$ surfactant films at the water-vacuum interface.[42] As such, we consider the SPC/E model adequate for the purposes of this study. For investigations focused on nucleation and growth of hydrates, other water models would perhaps be better suited. In particular, the generation of TIP4P-like water models, e.g., TIP4P/Ew, TIP4P/Ice, and TIP4P/2005, provides a good description of fluid-solid and solid-solid equilibria of water, as well

View Article Online
DOI: 10.1039/C6CP03296F

as of the surface tension of water over a wide range of temperatures.[43] It has recently been shown that using the TIP4P/Ice model it is possible to observe the spontaneous nucleation and growth of methane hydrates using MD.[44] The potential parameters for chloride ions were taken from Dang and collaborators.[45] Non-bonded interactions were modeled by means of dispersive and electrostatic forces. Electrostatic and dispersive interactions were described by the Coulombic and the 12-6 Lennard-Jones potentials, respectively. The Lennard-Jones parameters for unlike interactions were determined by the Lorentz-Berthelot mixing rules[46] from the values of like components. The cutoff distance for all interactions was set to 9 Å. Long-range corrections to electrostatic interactions were treated using the Particle Mesh Ewald (PME) method.[47] The simulated temperature was maintained at 277 K by Nose-Hoover thermostat[48,49] with a relaxation time of 100 fs. The equations of motion were solved by implementing the leapfrog algorithm[50] with 1.0 fs time steps.

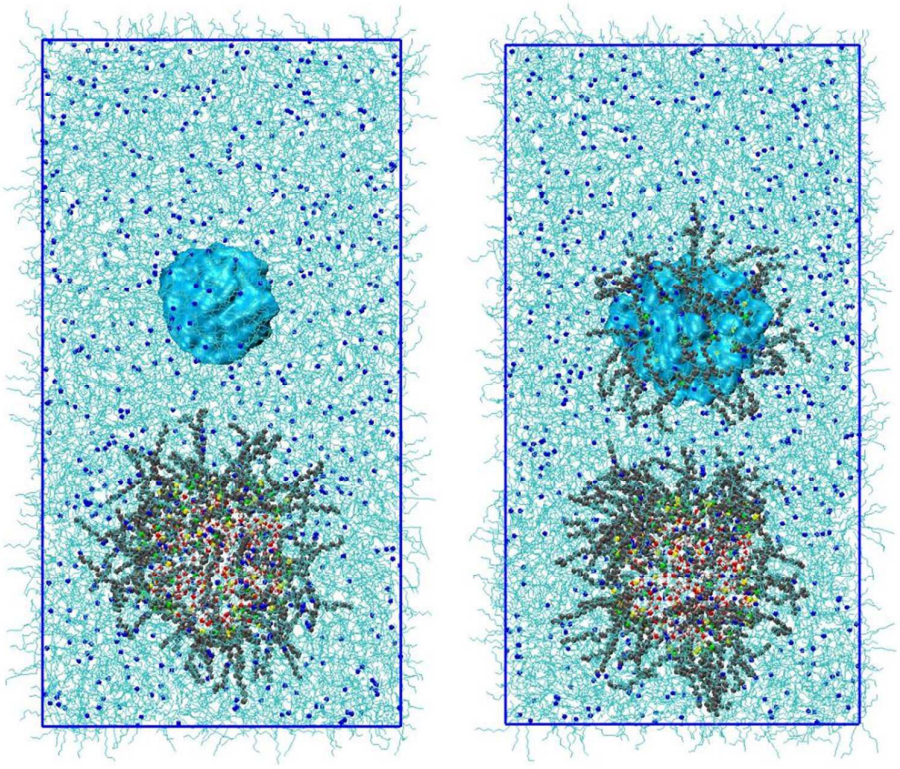

Figure 1. Representative simulation snapshots for systems containing one hydrate particle covered with surfactants and one bare water droplet (left) or one droplet coated with surfactants (right) immersed in a hydrocarbon mixture. A cyan spherical object represents the water droplet. Red and white spheres represent oxygen and hydrogen atoms in water molecules of hydrate, respectively. Yellow, green, and gray spheres represent chloride ions, nitrogen atoms and alkyl groups in surfactants, respectively. Blue spheres and cyan lines represent methane and n-decane molecules, respectively.

View Article Online
DOI: 10.1039/C6CP03296F

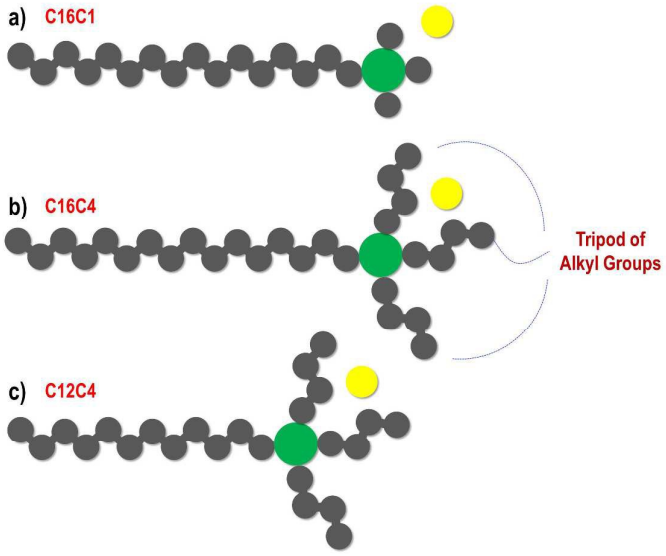

Figure 2. Chemical structures of (a) n-hexadecyl-trimethyl-ammonium chloride (C16C1), (b) n-hexadecyl-tri(n-butyl)-ammonium chloride (C16C4) and (c) n-dodecyl-tri(n-butyl)-ammonium chloride (C12C4). Chloride ions are modeled as completely dissociated. Yellow, green, and gray spheres represent chloride ions, nitrogen atoms and alkyl groups, respectively. The tripod of alkyl groups is highlighted in the figure.

We conducted steered MD simulations to mimic the hydrate coalescence as investigated by recent experimental approaches;[51-55] in our simulations the droplet was pulled towards the hydrate particle, which was maintained fixed. We used a harmonic spring with a force constant of 3000 kJ/mol.nm^2 tethered to the center of mass (COM) of the droplet. The COM position was pulled at a constant relative velocity (pulling rate). The results should depend on the pulling rate, with slower pulling rates expected to sample configurations more representative of equilibrated systems while requiring higher computing resources. For the system in which the water droplet was bare, we only used the pulling rate of 0.2 nm/ns, obtaining the expected results, used only as a reference in this work. For the systems in which the water droplet is covered by surfactants, we tested three pulling rates when the surfactant C16C1 was used: 0.2, 0.1, and 0.05 nm/ns. The individual force-distance curves are reported in Figure S1 of the Supplemental Material (SM), together with the approximate potentials of mean force (PMF) profiles. As expected, the results depend on the pulling rate, but the differences observed when the pulling rate was either 0.1 or 0.05 nm/ns were considered not very large. Because

View Article Online
DOI: 10.1039/C6CP03296F

the features of the hydrate-droplet force profiles are reminiscent of experimental observations we considered the pulling rate of 0.05 nm/ns a good compromise between computing costs and reliability of the results. All steered simulations discussed in the manuscript for water droplets covered by surfactants were conducted at the pulling rate of 0.05 nm/ns. It is worth noting that the steered velocities imposed in our simulations (0.2 or 0.05 m/s) are smaller than typical flow rates for water droplets in oil (~0.59 m/s),[56] suggesting that the method, although limited by computational limitations, should assess scenarios that have experimental relevance.

As one steered simulation progresses, the distance between the COM of the water droplet and that of the hydrate particle decreases, and eventually the two coalesce. The force exerted on the droplet by the spring was recorded every 20 time steps. The average droplet – hydrate particle COM-COM distance (D) during the 20 time steps was also recorded. To obtain one individual force – distance curve we conducted three independent steered simulations. We averaged the force obtained at each COM-COM distance to obtain the curves, such as those shown in Figure 3. More steered simulations for the same system should be conducted to reduce the large deviation between instantaneous forces and running averages. However, the individual force-distance curves (reported in Figure S2 and S3 of the SM) are qualitatively consistent with each other. Despite computing power limitations, we considered the results obtained sufficiently accurate to understand the molecular mechanisms of agglomeration. The simulated experiment was concluded when D decreased to ~ 2.1 nm. Coalescence is always reached, in the simulations discussed here, at distances D larger than this value.

View Article Online
DOI: 10.1039/C6CP03296F

Results and Discussion

A. Hydrate Particle – Droplet Coalescence

Force – Distance Profiles

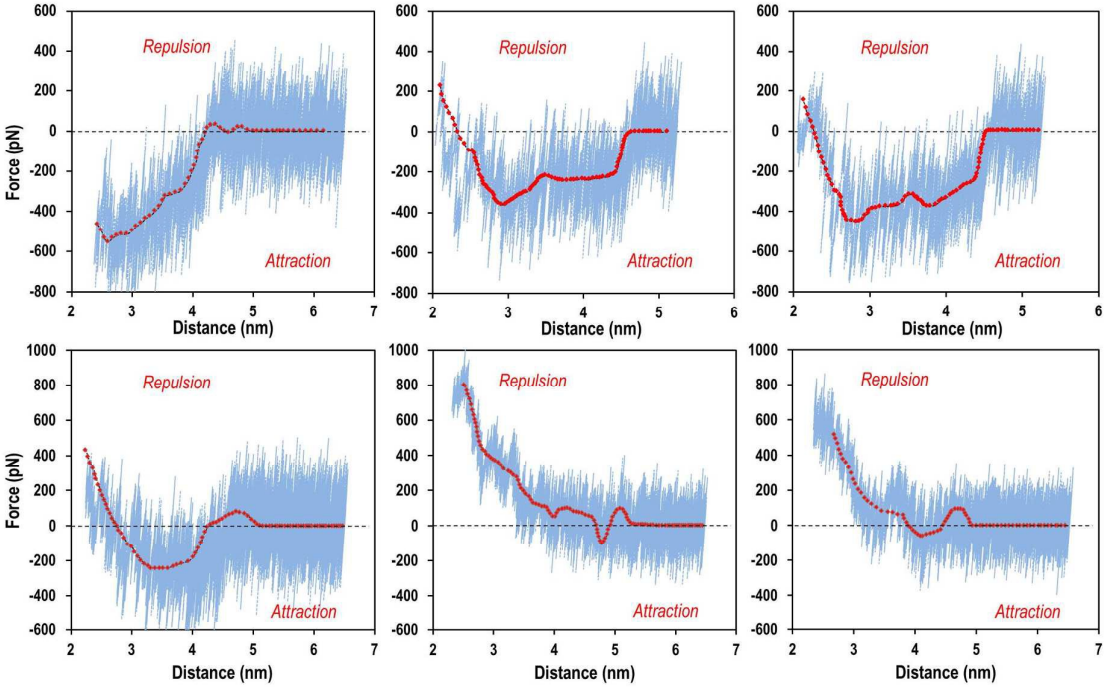

Figure 3. Simulated force-distance curves obtained while pulling the water droplet towards the hydrate particle. Results are shown for bare and coated water droplets (top and bottom panels, respectively). The surfactants used are C16C1 (left panels), C16C4 (middle panels) and C12C4 (right panels). Instantaneous forces (blue lines) and running averages (red lines) are both shown. The distance is that between the COM of the hydrate particle and that of the water droplet.

In Figure 3 we present the force profiles obtained as a function of the distance *D* between the COM of the water droplet and that of the hydrate particle during the steered simulations. While the hydrate particle is covered by surfactants in all cases, the water droplet is either bare (top panels) or coated (bottom panels). The surfactants considered are C16C1 (left panels), C16C4 (middle panels), and C12C4 (right panels). Visual inspection of representative simulation snapshots (see Figure S4 and S5 of the SM) combined with analysis of the force-distance profiles suggests that the force remains constant as long as the water droplet is not at contact with the hydrate particle. When the bare droplet begins to interact with the hydrate particle, the force decreases, indicating an effective attraction between the bare droplet and the hydrate particle, even though the latter is covered by surfactants.

View Article Online
DOI: 10.1039/C6CP03296F

This attraction starts at about $D \sim 4.1 - 4.5$ nm. One simulation snapshot obtained at this separation is reported in Figure S4 of the SM. The situation is different when the droplet is coated, in which case when the surfactants that cover the droplet come in contact with those covering the hydrate particle (at D ~ 4.5 – 5.3 nm), the force increases, indicating an effective repulsion due to the presence of surfactants on both interfaces. If strong enough, this repulsion could prevent coalescence, the goal of AAs in hydrates management. Our results suggest that the repulsive force reaches a local maximum at a distance that depends on the system considered, goes through a local minimum, and then increases monotonically as *D* continues to decrease. These qualitative force-distance profiles seem consistent with some such data reported experimentally. For example, Liu et al.[55] recently investigated the interactions between water droplet and cyclopentane hydrate particle covered by Span 80 surfactants using a micromechanical force (MMF) apparatus; Taylor et al.[57] and Aman et al.[58] used the MMF apparatus to study adhesion forces between hydrate particles in the presence of Span 20 and 80 surfactants, respectively. The experimental results are qualitatively similar to those we just described for the coated water droplet, although some differences need to be highlighted. These differences are due to the different sizes of the simulated vs. experimental systems. Both hydrate particles and water droplets are of size in the range of hundreds or thousands of microns in the experiments of Liu et al.[55] The interpretation of the experimental studies suggests that when hydrate particles are large (1-100 micron diameter) the AAs can help preventing water adsorption on the hydrates. When the hydrate particles are smaller, as in the conditions simulated here, it is expected that the surfactant layers contribute to yield an effective repulsion among hydrate particles. We point out that in all our simulations the results show that the force keeps increasing at short hydrate-droplet separations. This occurs because the droplet is forced to change its shape at the last stages of coalescence, which is consistent with the interpretation of experimental data.[55]

Qualitatively, the features just described are common in all simulated force – distance profiles obtained for the bare or the coated droplets, although different surfactants are considered. Some differences are however observed. For example, the distance *D* at which the water droplet (either bare or coated) begins to respond to the presence of the hydrate particle (i.e., when the force starts to either increase or decrease) using C16C1 is shorter than that for either C16C4 or C12C4 surfactants. Atomic

View Article Online
DOI: 10.1039/C6CP03296F

density profiles (see Figure S6 in the SM) suggest that this difference is due, at least in part, to the distribution of the chloride ions around the hydrate particle: these extend further away from the hydrate particle when either C16C4 or C12C4 surfactants are used rather than C16C1. The larger the distance of the ions from the particle is, the further away the water droplet responds to the presence of the hydrate. We also note that the effective attractive force experienced by the bare droplet as it approaches the hydrate particle covered with C16C1 is stronger than that obtained when using the other two surfactants. Consistently, we found that pulling the droplet coated with C16C1 surfactants towards the hydrate particle requires a weaker force than when using either one of the other two surfactants. These qualitative observations suggest that C16C4 and C12C4 act as more effective AAs than C16C1, which is consistent with experimental studies reported by Kelland et al.[10,15] These authors suggested that if the alkyl groups on the quaternary head group are shorter than the butyl groups, the tripod formed by these alkyl groups (see Figure 2) will more easily migrate on the hydrate surface, resulting in poor performance.

Approximate Pair Potentials of Mean Force

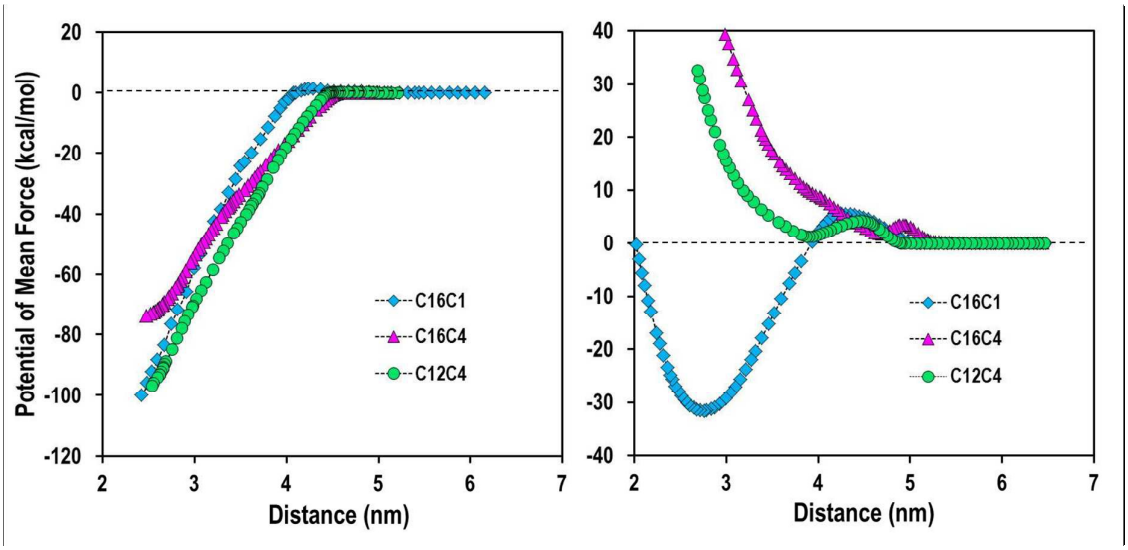

Figure 4. Approximate potentials of mean force plotted as a function of the distance between the COM of the hydrate particle and that of the water droplet. Results are shown for bare (left) and coated droplets (right panel). Different colors are for different surfactants: blue diamonds for C16C1, purple triangles for C16C4, and green circles for C12C4.

View Article Online
DOI: 10.1039/C6CP03296F

By numerically integrating the force profiles [$\langle F(z) \rangle$ along the z direction] shown in Figure 3, we can obtain the approximate effective potentials of mean force (PMF):[59]

$$PMF(z) = -\int_0^z \langle F(z') \rangle \, dz' \qquad (1)$$

We refer to this quantity as 'approximate' because the results of our procedure depend on the pulling rate, while the true PMF is an equilibrium property. Our PMF results are shown in Figure 4. The results shown in the left panel confirm that the interactions between the hydrate particle and the bare droplet lead to decreasing potential profiles as *D* decreases, suggesting an effective attraction between the bare water droplet and the hydrate particles covered by surfactants. No significant differences in the PMF are observed when using different surfactants, except those already discussed regarding the distance at which the force becomes attractive. The results on the right panel of figure 4 suggest that the PMFs between the hydrate particles and the coated droplets show a few common qualitative features: they are characterized by one moderately repulsive barrier at intermediate distances, a local minimum, and a monotonically increasing as *D* decreases. However, we point out that there is one significant difference in the PMFs as a function of the surfactant being simulated. Specifically, the effective particle – coated droplet PMF has a local minimum that is positive when C16C4 or C12C4 are used, and negative when C16C1 is used instead. The approximate PMF profiles obtained are therefore consistent with the interpretation according to which C16C4 and C12C4 are more effective AAs than C16C1. It is worth stressing that the results in either Figure 3 or Figure 4 do not show evidence of pronounced differences when either C16C4 or C12C4 are used.

Mechanism of Coalescence

To better understand the mechanism of coalescence, we conduct MD simulations for systems in which the hydrate particle remains fixed, and the water droplet is initially placed at a desired distance from the hydrate particle. The simulations are then conducted without steering the water droplet. We finally inspect the sequences of simulation snapshots to understand how the systems evolve under various scenarios. We repeated three times the simulations within initial configurations correspondent to the local maxima in the approximate PMF profiles. In all cases we obtained the same final configurations,

View Article Online
DOI: 10.1039/C6CP03296F

although the time needed by the trajectories to reach such final configurations differed. Thus the discussion below should be considered as qualitative in terms of time, and semi-quantitative in terms of mechanism of agglomeration.

In Figure 5 we present a sequence of simulation snapshots obtained for the system containing the hydrate particle coated with C16C1 surfactants and the bare droplet. The snapshots are collected at various stages during the simulation. From the initial configuration (t = 0 ns, panel A), the system evolves until the droplet touches the hydrate particle (t = 33.96 ns, panel B), and the coalescence is well underway (t = 35.86 ns, panel C). In other words, at the beginning of this simulation the droplet is far from the hydrate (D > 6 nm), and as the simulation progresses, it comes into contact with the hydrate, touches it, and merges with it. Although the surfactants were initially only present on the hydrate particle, they manage to re-distribute uniformly around the water-hydrate complex in ~ 21 ns after coalescence (t = 57.24 ns, panel D). This observation is important to confirm that the surfactants are mobile at the water-oil interface in our system. To confirm this further, we conducted a test simulation in which the surfactants were adsorbed densely on one region of a hydrate particle covered by a thin water film. The surfactants were found to distribute uniformly around the entire hydrate-water system in ~ 20 ns (see Figure S7 in SM). For completeness, it should be pointed out that our simulations suggest that the surfactants considered here hardly move when they are adsorbed on the hydrate surface without a thin water film present. While it is possible that allowing for atomic vibrations within the hydrate particle would permit noticeable surfactants diffusion, additional simulations, not reported here, suggest that a fully formed hydration layer might be necessary for observing lateral surfactants displacement in conventional atomistic molecular dynamics simulations.

The results shown in Figure 5 show that, even though the rather large number of C16C1 surfactants adsorbed on the hydrate surface are barely mobile, the bare water droplet is able to penetrate the protective surfactant film, and coalescence occurs. It appears that coalescence initiates when a molecularly thin water bridge forms between the droplet and the hydrate (a cyan sphere in Figure 5, Panel B, is used to highlight the first water molecule that is able to touch the hydrate particle after migrating from the water droplet). Once this bridge is formed, it widens, almost like a channel that

View Article Online
DOI: 10.1039/C6CP03296F

allows water molecules to transfer from the droplet to the surface of the hydrate, below the surfactants, the surfactants become mobile and they allow all of the water molecules to cover the hydrate particle. The same phenomena are observed when using either C16C4 or C12C4 as AAs (see Figure S8 in the SM).

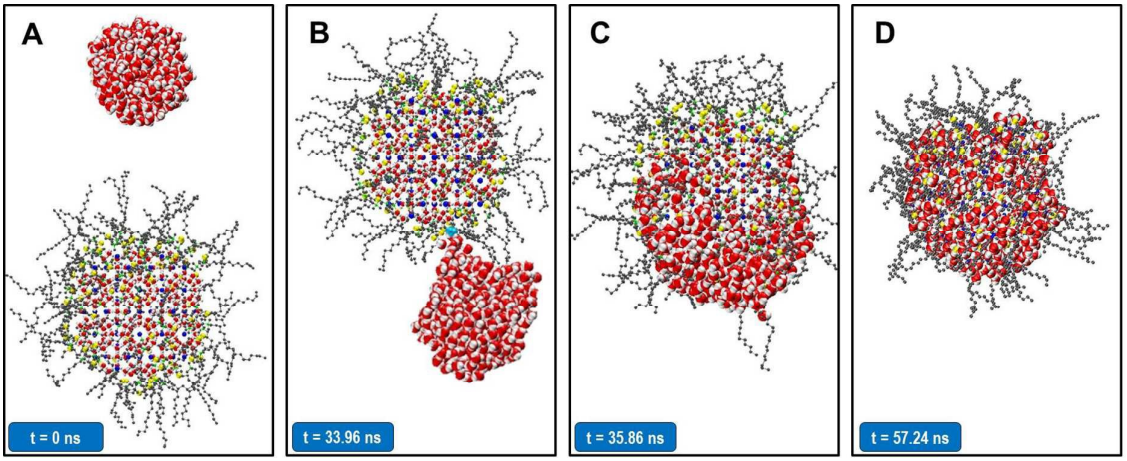

Figure 5. Sequence of simulation snapshots illustrating the coalescence between the hydrate particle and the bare water droplet. The simulations were conducted without steering forces. The images represent the evolution of the system from initial conditions (t = 0 ns, left), until the simulation is ended at t = 57.24 ns (right). Results are shown for C16C1 used as surfactant. The color code is the same as that of Figure 1, except that enlarged red and white spheres represent oxygen and hydrogen atoms in water molecules initially within the droplet. The hydrocarbon mixture is not shown for clarity. The cyan sphere in the middle panel highlights the first water molecule originally belonging to the droplet that manages to come in contact with the hydrate particle.

When we repeat a simulation similar to the one discussed in Figure 5 for a coated water droplet, we do not observe coalescence even after long simulation times (~ hundreds of nanoseconds), instead the water droplet moves further apart from the hydrate particle.

We used information from the approximate PMF, shown in Figure 4, to conduct simulations from 2 different initial configurations. The local maximum observed at D ~ 4.2 nm for the PMF on the right panel of Figure 4 (for C16C1 surfactants) should represent a kinetic barrier: when *D* is larger, the droplet and the particle should be repelled and move away from each other, when *D* is shorter the two should move closer to each other and coalesce, as expected by the theory of colloidal stability.[60] To test this, we initiated simulations from *D* = 4.2 nm (top panels in Figure 6) and from *D* = 4.18 nm (bottom panels in Figure 6). The sequence of simulation snapshots obtained when the initial

View Article Online
DOI: 10.1039/C6CP03296F

configuration is D = 4.2 nm shows that in 20 ns the coated droplet moves away from the hydrate particle, as expected. Clearly, the C16C1 surfactants on both hydrate and droplet prevent the agglomeration of Figure 5, within the time frame explored by our simulations.

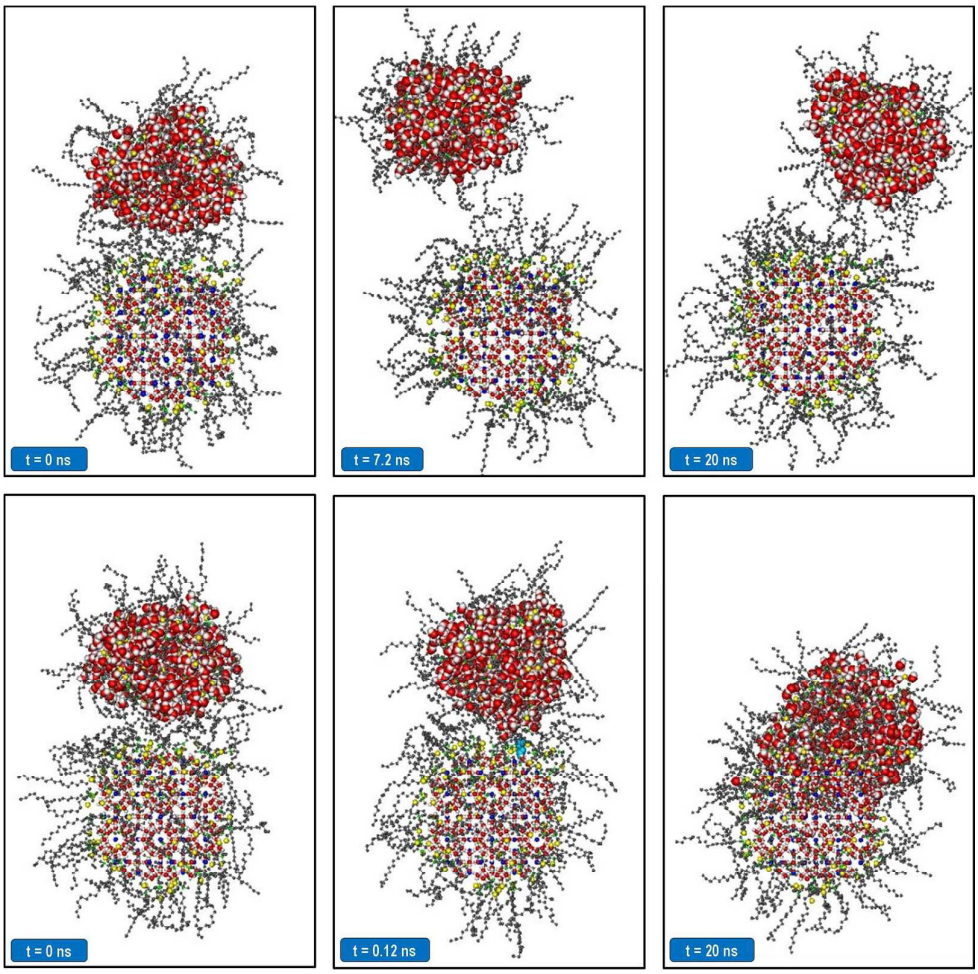

Figure 6. Same as Figure 5, but for the water droplet coated with C16C1 surfactants. Top and bottom panels represent two sequences of simulations started from slightly different initial configurations. *Top*: The initial configuration (left panel) is characterized by D = 4.2 nm, slightly larger than that correspondent to the local maximum in the PMF profile shown in Figure 4 (blue diamond data). *Bottom*: The initial configuration (left panel) corresponds to D = 4.18 nm, slightly shorter than the distance at which the PMF of Figure 4 shows the local maximum. In the bottom middle panel, at t = 0.12 ns, one water molecule (highlighted in cyan) establishes a molecular bridge between the hydrate particle and the droplet.

When the initial configuration is D = 4.18 nm, the simulation leads to coalescence within 20 ns of simulation (bottom panels in Figure 6). As observed in the case of the bare droplet, coalescence is initiated by one chain of water molecules that manages to build a bridge between the water droplet

View Article Online
DOI: 10.1039/C6CP03296F

and the hydrate particle; one water molecule is represented as a cyan sphere (middle bottom panel, Figure 6). It is perhaps surprising that this water bridge formed rather fast, within 0.12 ns from the start of the simulations. Once the bridge is formed, coalescence seems irreversible. After coalescence, the water molecules gradually spread over the hydrate surface and the surfactants uniformly redistribute as the simulation progresses further (not shown for brevity).

When C16C4 or C12C4 are used in our simulations, we observe coalescence when the simulations are initiated from a distance D closer than the mid-range repulsive barrier. In Figure S9 and S10 of the SM we show sequences of simulation snapshots obtained starting from $D \sim 4.9$ and 4.6 nm (C16C4 and C12C4 surfactants, respectively). In both cases, coalescence was observed. It is worth noting that the hydrate-droplet separation at which coalescence occurs spontaneously corresponds, approximately, to the sum of the radius of the water droplet and that of hydrate particle covered by chloride ions (see Table S1 of the SM), indicating that coalescence starts when water molecules touch the layer of chloride ions found on the hydrate particle (the chloride ions are often found near the surfactant head groups because of electrostatic interactions).

Visual observation of sequences of simulation snapshots (see Figure S11 of the SM) provides a significantly different result when C16C1 surfactants are simulated as opposed to either C16C4 or C12C4. Explicitly, when water droplet and hydrate particle merge the water molecules of the droplet are more likely to push away the C16C1 surfactants adsorbed on the hydrate surface than the other two surfactants. This is more pronounced at distances D correspondent to the local minimum in the PMF profile, which for C16C1 is highly negative, as shown in Figure 4.[61] This qualitative observation is consistent with the suggestions provided by Kelland et al., according to which it is more difficult to dislocate from the hydrate surface a tripod of butyl than one of methyl groups.[10,15]

The semi-quantitative results just described, as well as the quantitative PMF profiles discussed above, are expected to depend on the surface density of surfactants adsorbed on both hydrate particle and water droplet. If the surface density is significantly lower, the results in Figure 4 suggest that the surfactants would not be effective at preventing the agglomeration of water droplets and hydrate particles. On the other hand, while it would be expected that higher surface densities yield more effective stabilization, this may not necessarily be observed systematically. As the surfactant surface

View Article Online
DOI: 10.1039/C6CP03296F

density increases slightly compared to the conditions considered here, it is possible that the resultant denser film of self-assembled surfactants will both (a) induce a stronger repulsive interaction between water droplet and hydrate particle due to steric effects, as well as (b) make it more difficult for the water molecules to form a bridge between water droplet and hydrate particle. Both these effects are expected to more effectively prevent agglomeration. As the surfactant surface density increases further, the adsorbed films will eventually become thermodynamically unstable, and some of the surfactants would naturally desorb. This process could be investigated using coarse-grained models, but is at present beyond the capabilities of atomistic MD. Finally, it is possible that increasing the surfactant surface density above some optimal value could destabilize the surfactants adsorption on the hydrate particle. Because the simulation results suggest that anchoring of the surfactant headgroups on the hydrate is important for preventing agglomeration, this phenomenon would lead to less effective prevention of agglomeration. It is expected that the curvature of both water droplet and hydrate particle strongly affect the mechanisms just described, as it directly affects the surfactants ability to pack at an interface.[62] We are currently investigating systematically some of these phenomena.

B. Water Molecular Transport across the Hydrocarbon Phase

Free Energy Profiles

The results mentioned above highlight the importance of water molecules transferring through the protective film formed by the surfactants. To gain further insights into this process, we calculate the PMF for one tagged water molecule as it is displaced from the surface of the water droplet to the surface of the hydrate particle, across a thin film of hydrocarbon phase. For these calculations we implement the umbrella-sampling algorithm;[63,64] the computational details are reported in the SM. In these simulations a harmonic potential with force constant 3000 kJ/mol.nm^2 is used to keep the droplet at a distance D from the hydrate particle. It is worth repeating that only one individual water molecule is moved across the hydrocarbon film. The results are likely to depend on the surrounding molecules, both the surfactants and the hydrocarbon chains. To test this we considered the tagged water molecule at various positions in the XY plane (*dx* and *dy* represent the location of the water

View Article Online
DOI: 10.1039/C6CP03296F

trajectory from the COM of the hydrate particle in the plane perpendicular to the line connecting the COMs of water droplet and hydrate particle), as well as different distances *D* between hydrate particle and water droplet. The PMF results are shown in Figure 7 for systems containing C16C1 surfactants. Different colors represent results for different geometrical set ups. For the bare droplet (left panel) the results in blue are for *dx* = -0.08, *dy* = -0.16, *D* = 5.54 nm; the results in black are for *dx* = -0.03, *dy* = -0.04, *D* = 5.24 nm; the results in red are for *dx* = -0.15, *dy* = 0.19, *D* = 4.97 nm; and the results in green are for *dx* = -0.41, *dy* = -0.43, *D* = 5.24 nm. For the coated droplet (right panel) the results in blue are for *dx* = 0.03, *dy* = -0.44, *D* = 6.51 nm; and the results in red are for *dx* = 0.44, *dy* = -0.04, *D* = 6.01 nm. The PMF profiles shown on the left panel of Figure 7 have a similar shape: when the water molecule detaches from the droplet it encounters a relatively large free energy barrier as it migrates through the hydrocarbon phase; once the water molecule adsorbs on the hydrate particle, the PMF exhibits a minimum at *dz* ~ 2.2 nm. The results suggest that the PMF minimum depends on the distance *D* between water droplet and hydrate particle: our analysis of the interaction energies suggests that when the droplet is further from the hydrate the tagged water molecule is more strongly bound to the hydrate surface. Although the general shape of the PMF profiles follows the description just provided, different trajectories yield slightly different profiles. In particular, the PMF shown in green shows a local minimum that is located further away from the hydrate particle, shallower than those obtained for the other curves, and it also shows a small barrier close to the hydrate surface. This confirms that the effective water-hydrate interactions strongly depend on the location at which the water molecule adsorbs on the hydrate surface.

The results obtained when the water droplet is covered by surfactants are significantly different compared to those just discussed in the region near the hydrate particle. In fact, our calculations do not show pronounced local minima for the PMF obtained for the water molecule near the hydrate surface. Also, the PMF penalty experienced by the tagged water molecule as it is removed from the coated droplet and inserted into the hydrocarbon film is larger than that observed for the bare droplet (~8.2 vs. ~6.8 kcal/mol). It is possible that the presence of ammonium head groups and chloride ions in the droplet enhances the attraction between the tagged water molecule and the coated droplet.

View Article Online
DOI: 10.1039/C6CP03296F

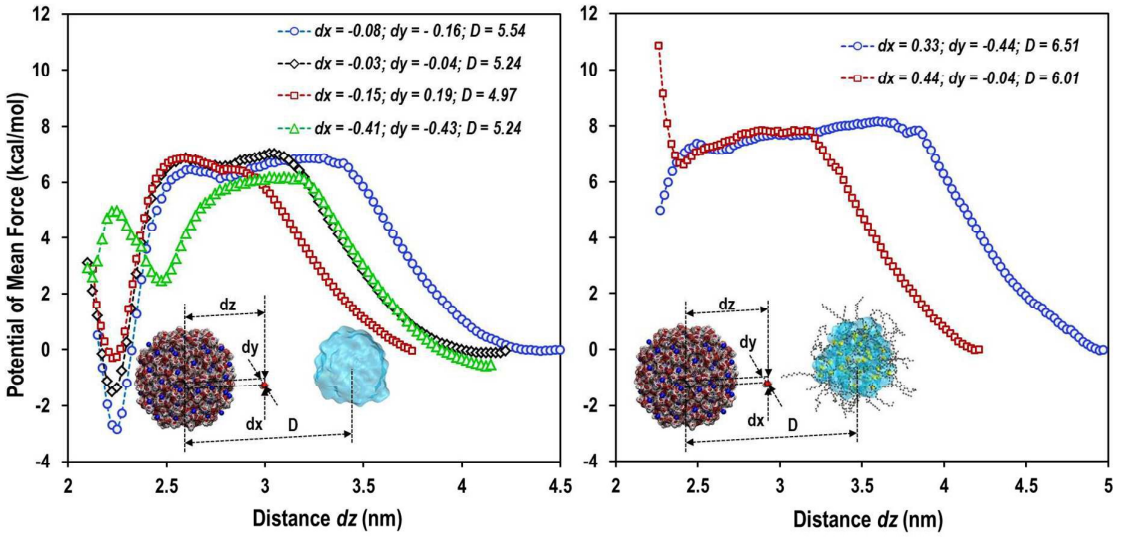

Figure 7. Potential of mean force calculated for one water molecule as it is moved from the water droplet (right side of each curve) to the hydrate particle (left). Results are obtained for the systems containing the hydrate particle coated with C16C1 surfactants and the bare (left panel) or coated droplet (right panel). The surfactants are not shown on the inset for clarity. The calculations are repeated for the tagged water molecule at various positions in the XY plane (*dx* and *dy* represent the location of the water trajectory from the COM of the hydrate particle in the plane perpendicular to the line connecting the COMs of water droplet and hydrate particle) and for the droplet located at various distances *D* from the hydrate particle.

Analysis of the simulations (see in-plane density distributions reported in Figure S12 of the SM) shows that the alkyl tails of C16C1 surfactants on the droplet disturb the hydrocarbon phase, which perhaps enables the tagged water molecule to travel faster.[65] It is possible that the correspondent disorder reduces the dispersive interactions between the water molecule and the hydrocarbon phase, and therefore increases the free-energy barrier experienced by the tagged water molecule.

In Figure 8 we report PMF results to compare the performance of different surfactants with regards to the ability of one water molecule to transfer across the hydrocarbon phase. Different colors are for different surfactants: blue, green, and purple are for C16C1, C16C4, and C12C4, respectively. In all cases the droplet is coated, and is located at D = 6.51 nm. In the left panel we quantify the effect of the quaternary head group (methyl vs. butyl). The results reveal that when the C16C1 surfactant is used the water molecule experiences a much stronger penalty when it is transferred into the hydrocarbon film than when C16C4 is used (~8.2 vs. 6.0 kcal/mol). It is likely that the butyl groups on the quaternary head group of C16C4 disturb the water – water hydrogen bond (HB) network in the droplet surface more strongly than the methyl groups and consequently weaken the water – droplet

View Article Online
DOI: 10.1039/C6CP03296F

effective interactions (as confirmed by results for the pair density profiles of water – ammonium and for the averaged number of HBs formed by a water molecule within the first hydration shell around ammonium head groups, shown in Figure S13 of the SM). This suggests the surfactants with the butyl tripod on the quaternary head group might be more capable of delaying hydrate growth when coalescence occurs.[66] In addition, as discussed above, it is difficult to displace the tripod of these alkyl groups from/on the hydrate surface. Both these observations suggest that the AA performance of C16C4 is much better than that of the C16C1.

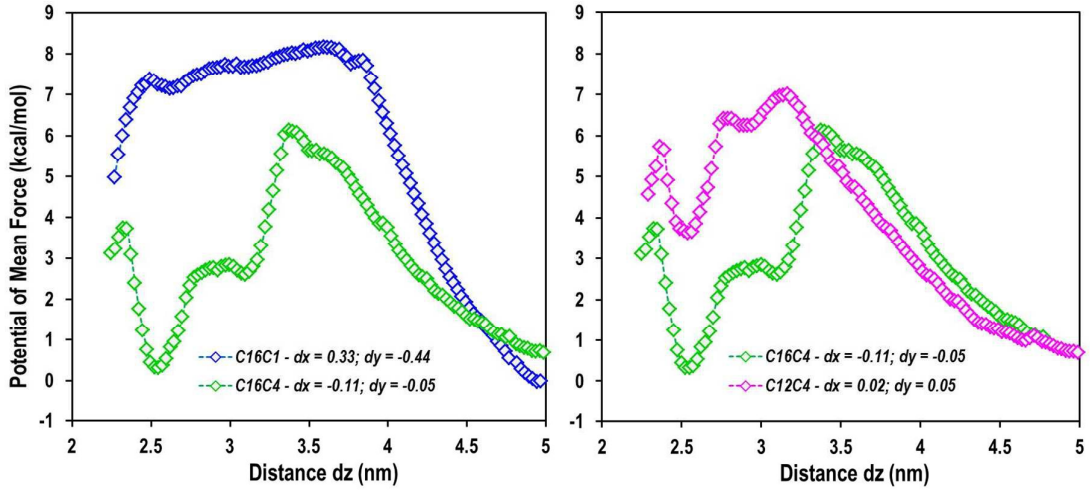

Figure 8. Same as Figure 7 for droplets coated with C16C1 (blue), C16C4 (green), and C12C4 (purple). In all cases the distance *D* between the hydrate particle and the water droplet is 6.51 nm.

In the right panel of Fig. 8 we compare the PMF profiles obtained in the presence of surfactants whose tails are of different lengths (C16C4 vs. C12C4). The PMF obtained in the presence of C12C4 shows a more intense PMF barrier and a shallower well as the water molecule approaches the hydrate surface. By analyzing the orientation of the surfactants hydrophobic tails (see Figure S14 in the SM), we found that C12C4 surfactants preferentially maintain their hydrophobic tails parallel to the hydrate surface; within this configuration, the surfactant tails cover much of the hydrate particle surface, and hence hinder the water molecule from adsorbing on the hydrate. Our results suggest that C12C4 surfactants yield a more compact protective film on the hydrate particle because the length of their hydrophobic tail (~12.2 Å) is comparable to that of the solvent considered in our simulations, n-

View Article Online
DOI: 10.1039/C6CP03296F

decane, ~ 9.97 Å. Similar effects due to the similarity between length of surfactants and length of solvent molecules were discussed previously.[67] Our PMF results, combined with analysis just summarized suggest that the water molecule transferred across the hydrocarbon phase is not favorably adsorbed on the hydrate surface. These results suggest that C12C4 is a more effective AA than C16C4, which is consistent with experimental results.[15] Our results seem to be consistent with the observations reported by Kelland et al.,[68] according to which the composition of the hydrocarbon phase could affect the AAs performance. It is possible that surfactants whose tail length is comparable with the length of the linear hydrocarbons in the system can act as effective AAs.

Rate of Water Transport – Diffusion Profiles

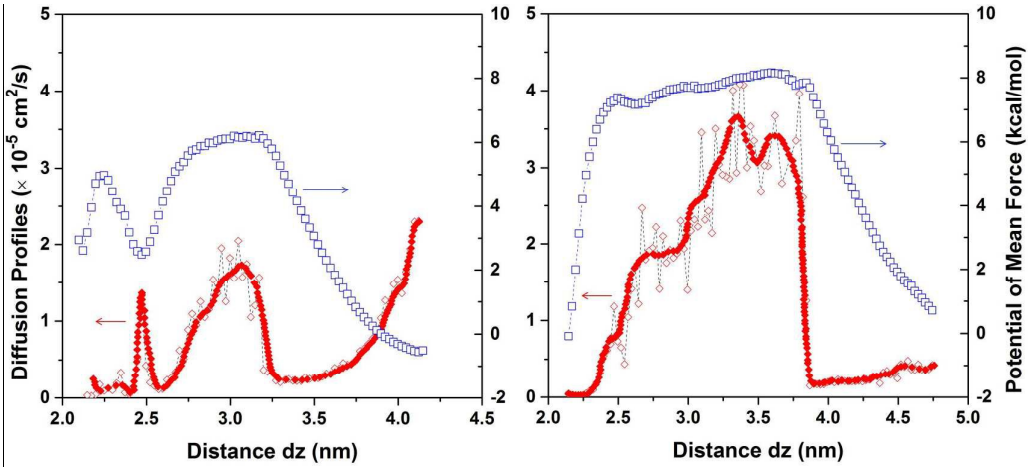

Figure 9. Local diffusion profiles (red diamonds) for the tagged water molecule travelling from the bare droplet located at *D* 5.24 nm (left panel) or from the coated droplet located at *D* 6.51 nm (right panel) to the hydrate particle. Results are obtained in the presence of C16C1. The correspondent PMF profile is reported using the blue squares.

Analysis of the umbrella sampling trajectories yields estimates regarding the local diffusion of the tagged water molecule as it desorbs from the water droplet, travels across the hydrocarbon film, and adsorbs on the hydrate surface. To extract this information we apply the formalism proposed by Woolf and Roux:[69,70]

$$\boldsymbol{D(dz = \langle dz \rangle)} = \frac{\boldsymbol{var(dz)}}{\boldsymbol{\tau_{dz}}} \quad , \qquad (3)$$

View Article Online
DOI: 10.1039/C6CP03296F

where $\langle dz \rangle$ is the average position of the harmonically restrained water molecule with respect to the COM of the hydrate particle along the Z direction, var(dz) = $\langle dz^2 \rangle$ - $\langle dz \rangle^2$ is its variance, and τ_{dz} is its correlation time, defined as

$$\boldsymbol{\tau_{dz}} = \frac{\int_0^\infty \langle \boldsymbol{\delta dz(t) \delta dz(0)} \rangle \boldsymbol{dt}}{\langle \boldsymbol{\delta dz^2} \rangle} \quad , \quad \text{with } \delta dz(t) = dz(t) - \langle dz \rangle \quad . \tag{4}$$

Representative results for the local diffusion profiles of the tagged water molecule are shown in Figure 9 (red diamonds), together with the correspondent PMF profiles (blue squares). The calculations are performed in the presence of C16C1. The results in general show that the local diffusivity of the tagged water molecule decreases as it leaves the water droplet, reaches a minimum and then increases within the hydrocarbon film, reaching a maximum not far from the hydrate particle. When the water molecule overcomes the PMF barrier and further approaches the hydrate surface its local diffusivity decreases. We observe a sharp peak in the local diffusivity profiles in correspondence of the local minima of the PMF near the hydrate surface. This is likely a signature of the ballistic motion of the water molecule as it approaches the local PMF minimum.[71] Comparing the results shown in Figure 9 (left vs. right panel), we observe that the local diffusivity of the tagged water molecule depends on whether the water droplet is covered by surfactant, as the diffusion results obtained at contact with the coated droplet (right panel) are much smaller than those found near the bare droplet (left panel). This might be a consequence of the quaternary ammonium and chloride ions embedded in the coated droplet because of the presence of the surfactants.[72] Regarding the results obtained when the droplet is bare (left panel), we also note that the diffusivity near the bare droplet (~ 2.0×10^{-5} cm^2/s) is somewhat comparable to the self-diffusion coefficient of bulk water at similar T and P conditions (1.3×10^{-5} cm^2/s).[73] Comparing the two panels, our results suggest that the tagged water molecule can diffuse faster within the hydrocarbon phase when the surfactants are present, probably because their alkyl tails disorder the hydrocarbon fluid, as mentioned above (note that the local diffusion within the hydrocarbon phase can reach ~3.5×10^{-5} cm^2/s in the presence of the coated droplet and only 1.8×10^{-5} cm^2/s in the presence of the bare droplet).

View Article Online
DOI: 10.1039/C6CP03296F

In Figure 10 we report the correspondent results obtained in the presence of various surfactants (C16C1, left, C16C4, middle, and C12C4, right). In all cases the water droplet is coated. The main qualitative features of the profiles have already been discussed. Varying the surfactant head groups does not seem to affect the local diffusivity of water. However, when the C16C1 surfactant is used, the tagged water molecule likely travels faster through the hydrocarbon phase than when the C16C4 and C12C4 surfactants are used. This might be due to the chloride ions, which are more likely found within the hydrocarbon phase when C16C4 or C12C4 surfactants are used rather than C16C1. It is possible that the chloride ions effectively hinder the movement of the tagged water molecule due to strong attractions between water and ions.

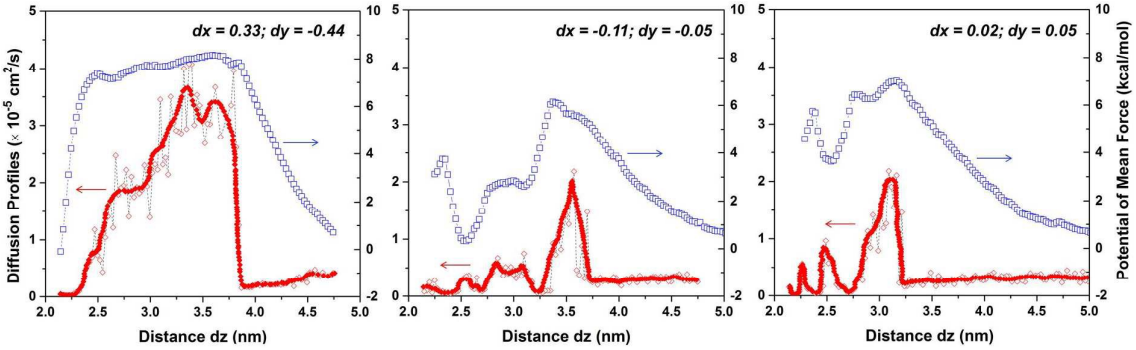

Figure 10. Same as Figure 9 in the presence of C16C1 (left panel), C16C4 (middle panel) and C12C4 (right panel).

Conclusions

We conducted steered and equilibrium molecular dynamics simulations to investigate the coalescence between one water droplet and one hydrate particle within a hydrocarbon phase. The simulations were conducted in the presence of various quaternary ammonium chloride surfactants. We quantified the effects due to varying the alkyl chain length (i.e., n-hexadecyl vs. n-dodecyl tails) and the alkyl groups on quaternary head group of the surfactants (e.g., methyl vs. butyl groups). Visual observation of sequences of simulation snapshots, as well as quantification of force-distance profiles indicate that the adsorption of surfactants on both the droplet and the hydrate particle can hinder the droplet from approaching the hydrate particle, therefore reducing the probability of agglomeration. The shapes of simulated force-distance profiles reported in this study are consistent with the ones from macroscopic experimental data. The results of force – distance profiles obtained from steered molecular dynamics

View Article Online
DOI: 10.1039/C6CP03296F

simulations and free energy profiles for individual water molecules travelling across the hydrocarbon phase from the water droplet to the hydrate particle, obtained implementing the umbrella sampling algorithm, both suggest that surfactants with butyl tripod on the quaternary head group and alkyl tail length similar to the solvent molecules could show good anti-agglomerant performance. Analysis of diffusion profiles for an individual water molecule pulled from the droplet towards the hydrate particle suggests strong effects due to the presence of surfactants on the local diffusivity of water, which could help understand the fundamental mechanisms responsible for the performance of anti-agglomerants under various conditions of experimental relevance in flow assurance. In particular, our results suggest that to be effective in flow assurance applications, the anti-agglomerants should be present on both hydrate particles and water droplets; they should adhere strongly on the hydrate particle (for our systems adhesion was provided by the butyl tripod on the surfactant head groups); they should yield a protective film on the hydrates (this can occur when the length of the surfactant tails is comparable to that of the hydrocarbon in the liquid phase). Perhaps unexpectedly, our simulations also suggest that the film of anti-agglomerants on the hydrate should be able to prevent the formation of molecularly thin chains of water molecules connecting the hydrate to an approaching water droplet because once such a chain is formed coalescence between hydrate particle and water droplet is inevitable.

Associated Content

Electronic supplemental information (ESI) available.

Acknowledgements

A.P. and T.B. wishes to thank financial support from Halliburton and from the UK Engineering and Physical Sciences Research Council (EPSRC), under grant number EP/N007123/1. Generous allocations of computing time were provided by the University College London Research Computing Platforms Support (LEGION), the Oklahoma Supercomputing Center for Education and Research (OSCER) and the National Energy Research Scientific Computing Center (NERSC) at Lawrence

View Article Online
DOI: 10.1039/C6CP03296F

Berkeley National Laboratory. NERSC is supported by the DOE Office of Science under Contract No. DE-AC02-05CH11231.

References

(1) J. E. Dendy Sloan, C. Koh, A. K. Sum, A. L. Ballard, J. Creek, M. Eaton, J. Lachance, N. Mcmullen, T. Palermo, G. Shoup and L. Talley, *Natural Gas Hydrates in Flow Assurance*; Elsevier, 2011.

(2) J. E. Dendy Sloan and C. A. Koh, *Clathrate Hydrates of Natural Gases*; Third Edition ed.; CRC Press, Taylor & Francis Group: Boca Raton, 2008.

(3) B. A. Buffett, *Annu Rev Earth Pl Sc*, 2000, **28**, 477-507.

(4) K. A. Kvenvolden, *Rev Geophys*, 1993, **31**, 173-187.

(5) S. L. Miller and W. D. Smythe, *Science*, 1970, **170**, 531-&.

(6) I. Chatti, A. Delahaye, L. Fournaison and J. P. Petitet, *Energ Convers Manage*, 2005, **46**, 1333-1343.

(7) J. P. Kennett, K. G. Cannariato, I. L. Hendy and R. J. Behl, *Methane Hydrates in Quaternary Climate Change: The Clathrate Gun Hypothesis*; American Geophysical Union: Washington, DC, 2003.

(8) E. D. Sloan, Jr., *Nature*, 2003, **426**, 353-359.

(9) E. G. Hammerschmidt, *Ind Eng Chem*, 1934, **26**, 851-855.

(10) M. A. Kelland, *Energ Fuel*, 2006, **20**, 825-847.

(11) A. Perrin, O. M. Musa and J. W. Steed, *Chem Soc Rev*, 2013, **42**, 1996-2015.

(12) B. J. Anderson, J. W. Tester, G. P. Borghi and B. L. Trout, *J Am Chem Soc*, 2005, **127**, 17852-17862.

(13) U. C. Klomp, V. R. Kruka, R. Reijnhart and A. J. Weisenborn; S. O. Company, Ed. US, 1997; Vol. US5648575 A.

(14) V. Panchalingam, M. G. Rudel and S. H. Bodnar; I. Champion Technologies, Ed. US, 2008; Vol. US7381689 B2.

(15) P. C. Chua and M. A. Kelland, *Energ Fuel*, 2013, **27**, 1285-1292.

(16) M. R. Anklam, J. D. York, L. Helmerich and A. Firoozabadi, *Aiche J*, 2008, **54**, 565-574.

(17) S. Q. Gao, *Energ Fuel*, 2009, **23**, 2118-2121.

(18) Z. Huo, E. Freer, M. Lamar, B. Sannigrahi, D. M. Knauss and E. D. Sloan, *Chem Eng Sci*, 2001, **56**, 4979-4991.

(19) M. A. Kelland, T. M. Svartaas, J. Ovsthus, T. Tomita and K. Mizuta, *Chem Eng Sci*, 2006, **61**, 4290-4298.

(20) X. K. Li, L. Negadi and A. Firoozabadi, *Energ Fuel*, 2010, **24**, 4937-4943.

(21) M. W. Sun and A. Firoozabadi, *J Colloid Interf Sci*, 2013, **402**, 312-319.

(22) M. W. Sun, Y. Wang and A. Firoozabadi, *Energ Fuel*, 2012, **26**, 5626-5632.

(23) M. L. Zanota, C. Dicharry and A. Graciaa, *Energ Fuel*, 2005, **19**, 584-590.

(24) J. D. York and A. Firoozabadi, *J Phys Chem B*, 2008, **112**, 845-851.

(25) F. M. Agazzi, N. M. Correa and J. Rodriguez, *Langmuir*, 2014, **30**, 9643-9653.

(26) F. Ding and B. I. Yakobson, *J Phys Chem Lett*, 2014, **5**, 2922-2926.

(27) H. Fan and A. Striolo, *Soft Matter*, 2012, **8**, 9533-9538.

(28) S. Fujiwara, T. Itoh, M. Hashimoto and R. Horiuchi, *J Chem Phys*, 2009, **130**.

(29) M. Marchi and S. Abel, *J Phys Chem Lett*, 2015, **6**, 170-174.

(30) A. V. Sangwai and R. Sureshkumar, *Langmuir*, 2012, **28**, 1127-1135.

View Article Online
DOI: 10.1039/C6CP03296F

(31) B. Hess, C. Kutzner, D. van der Spoel and E. Lindahl, *J Chem Theory Comput*, 2008, **4**, 435-447.
(32) D. Van der Spoel, E. Lindahl, B. Hess, G. Groenhof, A. E. Mark and H. J. C. Berendsen, *J Comput Chem*, 2005, **26**, 1701-1718.
(33) A. Amararene, M. Gindre, J. Y. Le Huerou, W. Urbach, D. Valdez and M. Waks, *Phys Rev E*, 2000, **61**, 682-689.
(34) *Food Science and Food Biotechnology*; CRC Press: Taylor & Francis Group, 2003.
(35) M. G. Martin and J. I. Siepmann, *J Phys Chem B*, 1998, **102**, 2569-2577.
(36) W. L. Jorgensen and J. Gao, *J Phys Chem-Us*, 1986, **90**, 2174-2182.
(37) B. Smit, S. Karaborni and J. I. Siepmann, *J Chem Phys*, 1995, **102**, 2126-2140.
(38) H. J. C. Berendsen, J. R. Grigera and T. P. Straatsma, *J Phys Chem-Us*, 1987, **91**, 6269-6271.
(39) S. Miyamoto and P. A. Kollman, *J Comput Chem*, 1992, **13**, 952-962.
(40) N. R. Tummala, S. Liu, D. Argyris and A. Striolo, *Langmuir*, 2015, **31**, 2084-2094.
(41) M. Suttipong, N. R. Tummala, A. Striolo, C. S. Batista and J. Fagan, *Soft Matter*, 2013, **9**, 3712-3719.
(42) L. Shi, N. R. Tummala and A. Striolo, *Langmuir*, 2010, **26**, 5462-5474.
(43) C. Vega and E. de Miguel, *J Chem Phys*, 2007, **126**.
(44) L. Jensen, K. Thomsen, N. von Solms, S. Wierzchowski, M. R. Walsh, C. A. Koh, E. D. Sloan, D. T. Wu and A. K. Sum, *J Phys Chem B*, 2010, **114**, 5775-5782.
(45) D. E. Smith and L. X. Dang, *J Chem Phys*, 1994, **100**, 3757-3766.
(46) M. P. Allen and D. J. Tildesley, *Computer Simulation of Liquids*; Oxford University Press: Oxford, UK, 2004.
(47) U. Essmann, L. Perera, M. L. Berkowitz, T. Darden, H. Lee and L. G. Pedersen, *J Chem Phys*, 1995, **103**, 8577-8593.
(48) W. G. Hoover, *Phys Rev A*, 1985, **31**, 1695-1697.
(49) S. Nose, *Mol Phys*, 1984, **52**, 255-268.
(50) R. W. Hockney, S. P. Goel and J. W. Eastwood, *J Comput Phys*, 1974, **14**, 148-158.
(51) Z. M. Aman, K. Olcott, K. Pfeiffer, E. D. Sloan, A. K. Sum and C. A. Koh, *Langmuir*, 2013, **29**, 2676-2682.
(52) J. H. Song, A. Couzis and J. W. Lee, *Langmuir*, 2010, **26**, 9187-9190.
(53) Z. M. Aman, E. D. Sloan, A. K. Sum and C. A. Koh, *Phys Chem Chem Phys*, 2014, **16**, 25121-25128.
(54) Z. M. Aman, W. J. Leith, G. A. Grasso, E. D. Sloan, A. K. Sum and C. A. Koh, *Langmuir*, 2013, **29**, 15551-15557.
(55) C. W. Liu, M. Z. Li, G. D. Zhang and C. A. Koh, *Phys Chem Chem Phys*, 2015, **17**, 20021-20029.
(56) S. Papavinasam, *Corrosion Control in the Oil and Gas Industry*; Gulf Professional Publishing, 2014.
(57) C. J. Taylor, L. E. Dieker, K. T. Miller, C. A. Koh and E. D. Sloan, *J Colloid Interf Sci*, 2007, **306**, 255-261.
(58) Z. M. Aman, L. E. Dieker, G. Aspenes, A. K. Sum, E. D. Sloan and C. A. Koh, *Energ Fuel*, 2010, **24**, 5441-5445.
(59) F. Lo Verso, L. Yelash, S. A. Egorov and K. Binder, *J Chem Phys*, 2011, **135**.
(60) J. Rossi and J.-C. Leroux, In *Role of Lipid Excipients in Modifying Oral and Parenteral Drug Delivery: Basic Principles and Biological Examples*; K. M. Wasan, Ed.; John Wiley & Sons, Inc.: Hoboken, NJ, 2006.
(61) S. C. Lin, A. J. Hilmer, J. D. Mendenhall, M. S. Strano and D. Blankschtein, *J Am Chem Soc*, 2012, **134**, 8194-8204.
(62) N. R. Tummala and A. Striolo, *Phys Rev E*, 2009, **80**.
(63) G. M. Torrie and J. P. Valleau, *Chem Phys Lett*, 1974, **28**, 578-581.

View Article Online
DOI: 10.1039/C6CP03296F

(64) G. M. Torrie and J. P. Valleau, *J Comput Phys*, 1977, **23**, 187-199.
(65) S. Riahi and C. N. Rowley, *J Am Chem Soc*, 2014, **136**, 15111-15113.
(66) Y. M. Makogon and E. D. Sloan In *Proceedings of the 4th International Conference on Gas Hydrates* Yokohama, Japan, 2002, p 498-503.
(67) S. S. Jang, S. T. Lin, P. K. Maiti, M. Blanco, W. A. Goddard, P. Shuler and Y. C. Tang, *J Phys Chem B*, 2004, **108**, 12130-12140.
(68) M. A. Kelland, A. Grinrod and E. G. Dirdal, *J Chem Eng Data*, 2015, **60**, 252-257.
(69) T. B. Woolf and B. Roux, *J Am Chem Soc*, 1994, **116**, 5916-5926.
(70) G. Hummer, *New J Phys*, 2005, **7**.
(71) F. Sedlmeier, Y. von Hansen, L. Mengyu, D. Horinek and R. R. Netz, *J Stat Phys*, 2011, **145**, 240-252.
(72) K. Tanaka, *J Chem Soc Farad T 1*, 1984, **80**, 2563-2566.
(73) R. Mills, *J Phys Chem-Us*, 1973, **77**, 685-688.